Detection of Cavitation in a Venturi Injector With a Combined Method of Strain Gauges and Numerical Simulation

Yuncheng Xu
College of Water Resources and Civil Engineering, China Agricultural University, Beijing 100083, China
e-mail: ycxu1990@gmail.com

Yan Chen
College of Water Resources and Civil Engineering, China Agricultural University, Beijing 100083, China
e-mail: caihua2008@yeah.net

Jianqiang He
College of Water Resources and Architectural Engineering, Northwest A&F University, Shaanxi 712100, China
e-mail: mythbird@hotmail.com

Haijun Yan[1]
College of Water Resources and Civil Engineering, China Agricultural University, Beijing 100083, China
e-mail: yanhj@cau.edu.cn

The fertilizer suction capability of a Venturi injector is dependent on the vacuum pressure in the throat portion. As the vacuum level drops below the saturation vapor pressure, the pressure decreases to a particular value corresponding to the maximum pressure difference (Δp_{max}) between inlet and outlet pressures, and critical cavitation is likely to occur, leading to an unstable suction flow rate and low fertilization uniformity. A new method of using strain gauges to detect cavitation in Venturi injectors was explored experimentally and verified numerically under various operating conditions. The standard deviation (SD) of the measured strain values and the simulated values of the vapor-phase volume fraction (V_f) were used to evaluate the influence of cavitation. The results showed that both the rate of increase (η_m) of the average SD and the average growth rate (AGR) of the simulated cavitation length reach relatively large values at the maximum pressure difference (Δp_{max}), where the measured suction flow rate simultaneously reaches a maximum. In addition, SD and V_f shared similar variation trends at pressure differences larger than the corresponding Δp_{max} under various conditions. This new cavitation detection method has been proved to be feasible and reliable. It helps to determine accurately the value of Δp_{max} at different inlet pressures and to ensure that the Venturi injector runs in a safe operating-pressure range. [DOI: 10.1115/1.4026879]

Keywords: Venturi injector, cavitation, detection, strain gauge, numerical simulation

1 Introduction

With the growing shortage of water resources and increasing investment in agricultural infrastructure, high-efficiency water-saving irrigation technology has become very popular in China. According to the statistical bulletins of the Chinese government [1], the national area under water-saving irrigation has increased from 16.0 to 28.7×10^6 hm^2 during the period from 2000 to 2011. Because fertilization technology in drip irrigation systems has enabled high yield, quality, and efficiency in crop production [2], the application area of this technology had increased to 2×10^6 hm^2 by the end of 2011 in China. Among all kinds of fertilizer injection devices, the Venturi injector has been widely used in drip irrigation systems due to its distinct advantages of simple structure, convenient operation, and not needing an extra power supply [2,3].

Unlike the well-known Venturi tube, the Venturi injector has a suction orifice in its throat portion that is connected to a fertilizer solution tank by a flexible pipe. The suction capability for fertilizer solution was found to be dependent on the pressure and vacuum level in the throat portion of the Venturi injector. The suction flow rate increases with increasing inlet pressure (p_1) and increasing difference between inlet and outlet pressure (Δp) [4]. In practice, a minimum pressure difference ($\Delta p_{\min}$) is required to initiate suction at a given inlet pressure. However, as the vacuum level reaches a certain value below the saturated vapor pressure, critical cavitation may occur, which dramatically affects the internal flow patterns in the Venturi injector [5]. Abrasion caused by critical cavitation in the minimum-diameter point of the Venturi injector throat could lead to reduction of the suction flow rate for given operating conditions and eventually affect fertilization uniformity and drip-irrigation system efficiency. Therefore, a Venturi injector should function within an appropriate operating-pressure range to prevent critical cavitation. Predicting and detecting the occurrence of critical cavitation therefore becomes an important issue in Venturi injector design and operation.

Recently, researchers have studied cavitation in Venturi injectors and its relationship to injection characteristics and structural parameters. Jing et al. [6] found that when the flow-rate ratio (ratio of suction flow rate to outlet flow rate) was greater than 10%, cavitation initially occurred in the Venturi injector and the corresponding pressure ratio (ratio of inlet pressure to outlet pressure) decreased rapidly. Yan et al. [7] found that if the flow-rate ratio exceeded a certain value, the injection capacity appeared to become unstable and even to decrease. Barre et al. [8] studied Venturi tubes with diffusion angles of 4 deg and 8 deg and found that cavitation varied periodically for a diffusion angle of 8 deg and occurred with small fluctuations for a diffusion angle of 4 deg. Ardiansyah et al. [9] reported that cavitation accelerated abrasion on the internal surface of a Venturi tube.

In fluid engineering, several methods are used for cavitation detection, including photographic methods, coating corrosion, static-pressure measurement, and vibration measurement [10]. Cudina et al. [11] used noise changes to analyze cavitation initiation in pumps. They found a strong correlation between the length of discrete noise within the audible wavelength and cavitation development. Pu et al. [12] and Liu et al. [13] explored a method based on wavelet entropy for cavitation initiation monitoring and status identification. Al-Hashmi [14] used both noise signals and

[1]Corresponding author.

Contributed by the Fluids Engineering Division of ASME for publication in the JOURNAL OF FLUIDS ENGINEERING. Manuscript received March 29, 2013; final manuscript received February 17, 2014; published online May 15, 2014. Assoc. Editor: Olivier Coutier-Delgosha.

vibration signals recorded by an accelerometer to analyze cavitation in centrifugal pumps. In his study, SD and probability density distribution were calculated to analyze the vibration signal. Yazici et al. [15] used high-speed cinematography and particle-image velocimetry (PIV) techniques to demonstrate bubble shedding and cavitation processes in a transparent Venturi tube. However, few studies on cavitation detection in Venturi injectors are available in the recent literature. For Venturi injectors made of nontransparent plastics, it is impossible to observe internal flow using imaging and PIV techniques. It is also difficult to use vibration measurement because it is impractical to put an accelerator sensor on a Venturi injector. In addition, cavitation detection in Venturi injectors using acoustic techniques may be disturbed by ambient noise, leading to inaccurate results [10].

During the short period of initiation, increase, and collapse of cavitation bubbles, the induced energy transformation can impact the internal surface of a Venturi injector and lead to body deformation caused mainly by imposed bending moment. Bending-moment variation can be accurately measured with strain gauges that are directly attached onto the external surface of an object for detection without any damage to object structures. The bending-moment variation can reflect the influence of cavitation on the body [16–18]. Hence, a new method of cavitation detection in Venturi injectors using strain gauges was initially proposed in the present study. In addition, numerical simulation using the FLUENT software was also carried out under the same experimental conditions to verify to a certain extent the measurement accuracy of this new detection method because other available direct-detection methods could not be used in this situation. Although few papers have been found on numerical simulation of cavitation in Venturi injectors, a certain number of publications related to similar fluid instruments (e.g., Venturi nozzles, inducers, tubes, and so forth) are available [19–23]. These scientific findings can help to develop a numerical simulation of cavitation in a Venturi injector.

The main objectives of this study were: (1) to explore and test a new method for cavitation detection in Venturi injectors based on strain gauges and (2) to verify this new method through numerical simulation using the FLUENT software. This study provides a simple way to determine accurately the maximum pressure value (Δp_{max}) which corresponds to critical cavitation in a Venturi injector.

2 Materials and Methods

2.1 Structure of a Venturi Injector. The Venturi injector (Fig. 1) studied here had an inlet diameter of 15.6 mm, an outlet diameter of 22 mm, and a minimum diameter of 4 mm in the throat-constriction portion. It was made of acrylonitrile butadiene styrene (ABS) plastic, with wall thicknesses of 3.0 mm at the throat portion and 7.8 mm at the diffusion portion, which is a little thicker than products currently on the market.

2.2 Cavitation Detection Based on Strain Gauges

2.2.1 Experiment Setup and Procedures. The experiment was conducted at the College of Water Resources and Civil Engineering, China Agricultural University. The Venturi injector was installed horizontally (Fig. 2). All connected pipes were made of unplasticized polyvinyl chloride (UPVC). The inner diameter of the main pipes was 36 mm. The inner upstream and downstream diameters of the Venturi injector were 21 mm and 28 mm, respectively. A flexible 8-mm-diameter pipe, through which the fertilizer solution could be injected, was connected to the suction orifice. Two turbine flow meters (types LWGY-15 and LWGY-25; components 4 and 8 in Fig. 2) were installed on the upstream and downstream pipes to measure inlet and outlet flow rates. The suction flow rate (Q_3) was calculated by subtracting the inlet flow rate (Q_1) from the outlet flow rate (Q_2). Two pressure gauges (components 5 and 7 in Fig. 2) were installed to control inlet and outlet pressures in the Venturi injector. Clean water was used to replace fertilizer solution in the supply tank during the test. The vertical distance between the axis line of the Venturi injector and the water level in the supply tank was maintained at 350 ± 10 mm during the whole experiment using a water supply pipe with a continuous water supply.

Two pairs of strain gauges were attached to the external surfaces of the throat and the diffusion portion of the Venturi injector. Each pair was symmetric to the axis line of the Venturi injector and was connected to a dynamic strain indicator by a half-bridge (Fig. 1). The *X*-axis of the coordinate system coincided with the center line of the injector inlet and outlet, while the *Y*-axis coincided with the center line of the suction orifice. Dynamic strain indicators were used to measure strain values in the throat and diffusion portions simultaneously. The variations in the strain signals were expected to reflect changes in the internal flow inside the Venturi injector.

Various experimental scenarios were implemented by adjusting the valves in the experimental system. According to actual operating conditions, inlet pressure was set to 0.15, 0.20, 0.25, 0.30, 0.35, 0.40, and 0.45 MPa. While keeping inlet pressure at a given constant value, outlet pressure was gradually decreased from the suction-initiation outlet pressure by steps of 0.025 MPa to create the required pressure difference. According to the authors' experience, when a rapidly rising noise was heard, critical cavitation was assumed to be occurring. Then the pressure decrement was adjusted to 0.01 MPa to achieve more informative and accurate detection. In each scenario, two 1000-Hz channels in the dynamic strain indicator were used to record the strain signals for at least 20 s.

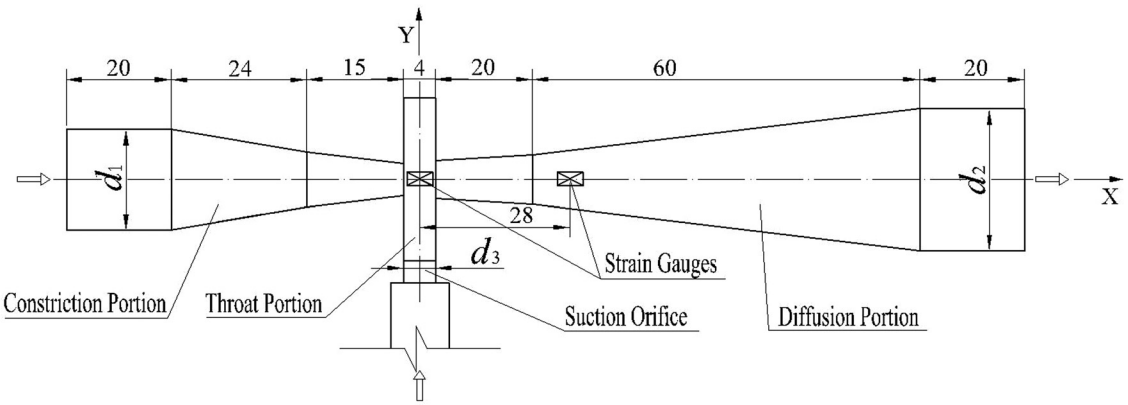

Fig. 1 Internal structure of the Venturi injector with strain gauges attached to its surface. Dimensions in millimeters (mm).

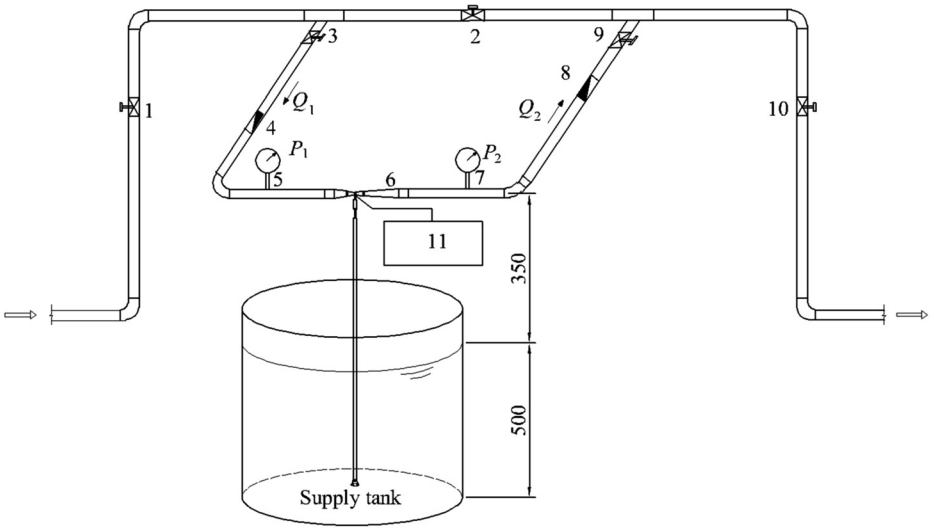

Fig. 2 Schematic diagram of experimental device for cavitation detection in a Venturi injector, including valves (components 1, 2, 3, 9, and 10), turbine flow meters [4,8], pressure gauges [5,7], a Venturi injector with strain gauges attached [6], and a dynamic strain indicator [11]. Dimensions in millimeters (mm).

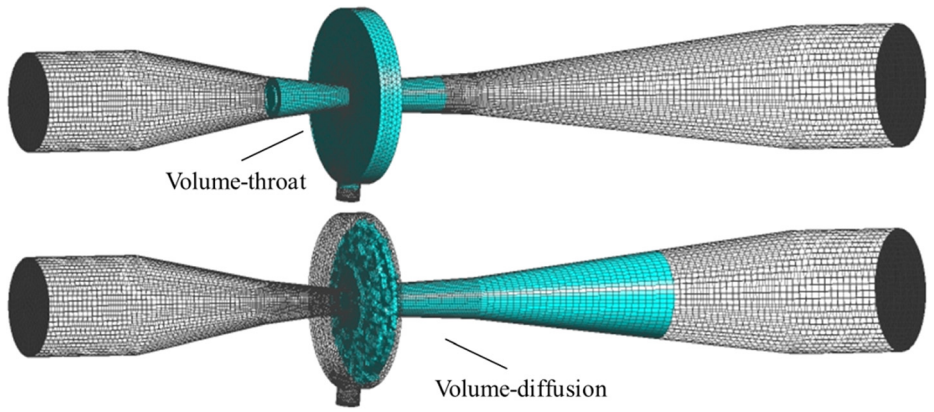

Fig. 3 Schematic views of volume–throat and volume–diffusion domains. The blue volumes represent the computational domains of the two spherical volumes.

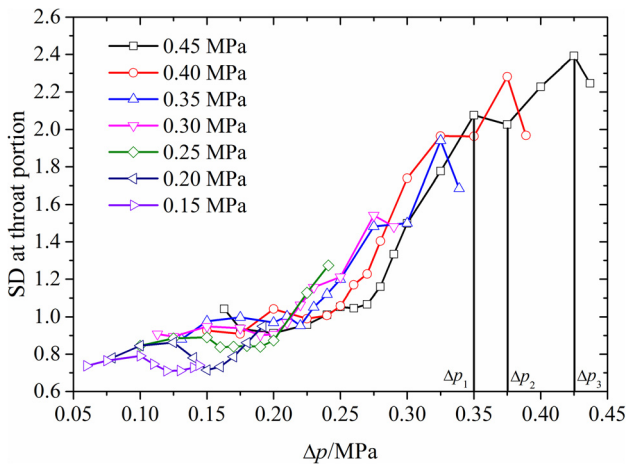

Fig. 4 Relationship between SD of strains at the throat portion of the Venturi injector and the pressure differences (Δp) under seven different inlet pressures. Vertical lines of Δp_1, Δp_2, and Δp_3 correspond to an inlet pressure of 0.45 MPa.

2.2.2 Statistical Indicators. Strain values over a period of 20 s, or 20,000 values for each channel, were obtained for each scenario. The standard deviation of the 20,000 values was calculated using the following formula:

$$\mathrm{SD} = \sqrt{\frac{1}{n}\sum_{i=1}^{n}(\varepsilon_i - \bar{\varepsilon})^2} \tag{1}$$

where ε_i is the ith strain value in the 20-s period, $\bar{\varepsilon}$ is the average value of all strain values in the 20-s period and SD. As an eigenvalue of these 20,000 strain values, the value of SD reflects the degree of deformation in the throat and diffusion portions.

The rate of increase (η_m) of the average SD was calculated as follows:

$$\eta_m = \frac{\mathrm{SD}_m - \frac{1}{m-1}\sum_{j=1}^{m-1}\mathrm{SD}_j}{\frac{1}{m-1}\sum_{j=1}^{m-1}\mathrm{SD}_j} \times 100\% \tag{2}$$

where SD_1 is the first SD value measured for each inlet pressure which corresponds to suction initiation; SD_j is the value of SD in

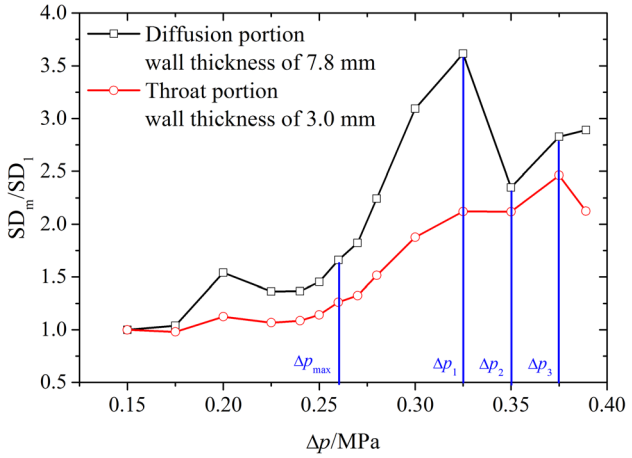

Fig. 5 Relationship between the SD ratio (SD_m/SD_1) at the throat portion and the diffusion portion and the pressure difference (Δp) at an inlet pressure of 0.40 MPa. Three eigenvalues, Δp_1, Δp_2, and Δp_3. Maximum pressure difference Δp_{max}.

the jth scenario for each inlet pressure; and η_m is assumed to be approximately zero when only slight deformations are occurring in the throat and diffusion portions, but to increase suddenly when large deformations caused by violent cavitation occur at these locations.

2.3 Numerical Simulation. To verify the experimental results for the SD of the strain values, numerical simulations of cavitation in a Venturi injector were conducted using the FLUENT software. The setup of some of the basic models required in the simulation can be briefly summarized as follows.

2.3.1 Turbulence Model. The two-equation k-ε models which are widely used worldwide were selected as the turbulence model in the present study. A preliminary comparison of three basic k-ε models, including standard k-ε, RNG k-ε, and realizable k-ε, indicated that the convergence rate of the standard k-ε model could reach 10^{-5} after 7000 iterations, but was only 10^{-3} for the other two models after the same number of iterations. Therefore, the standard k-ε model was used in this study. The relevant simulation constants were $C_{1\varepsilon}=1.44$, $C_{2\varepsilon}=1.92$, $C_\mu=0.09$, $\sigma_k=1.0$, $\sigma_\varepsilon=1.3$ [24].

2.3.2 Cavitation Model. The FLUENT software module offers three cavitation models: the Schnerr and Sauer model [25], the Singhal model [26], and the Zwart–Gerber–Belamri model [27]. The Schnerr and Sauer model has been used for cavitation simulation of Laval and injection nozzles, which are structurally similar to Venturi injectors, and obtained good simulation results [28,29]. Therefore, this model was used in this study. This model includes an exact expression of net mass transfer from liquid to vapor. The only parameter that needs to be determined is the number of spherical bubbles per volume of liquid. In the simulation, liquid water was set as the first phase and water vapor as the second. It was assumed that there was no heat transformation, mass transfer, or slide between these two phases. The vaporization pressure constant was 3540 Pa, and the bubble density was 10^{13}.

2.3.3 Computational Mesh. Geometric modeling and mesh generation for the internal computation domain of the Venturi injector were conducted using the Gambit software. The domain was separated into three portions: constriction, throat, and diffusion. The constriction and throat portions were respectively meshed using a Cooper grid with a density of 0.4 mm and a T grid grid with a density of 1 mm. For the front of the diffusion portion, a boundary layer 0.1 mm in thickness was defined to obtain better

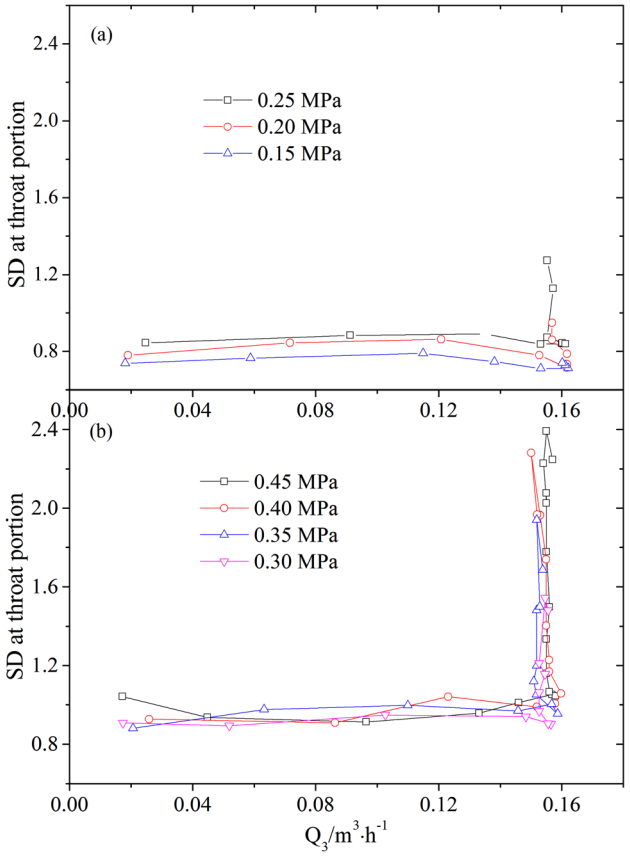

Fig. 6 Relationship between SD of strain values at the throat portion and suction flow rate (Q_3) at inlet pressures of (*a*) 0.30–0.45 MPa and (*b*) 0.15–0.25 MPa

computational precision. The whole computation domain contained a total of 152,932 grid cells and 108,605 nodes.

2.3.4 Boundary Conditions. Velocity boundaries were defined at both inlet and suction orifices of the Venturi injector. Initial inlet and suction velocities (v_1 and v_3) could be calculated as follows:

$$v_1 = 4Q_1/(\pi d_1^2) \tag{3}$$

$$v_3 = 4Q_3/(\pi d_3^2) \tag{4}$$

where Q_1 and Q_3 are the measured inlet and suction flow rates under a given scenario and d_1 and d_3 are the diameters of the inlet and suction orifices respectively.

The pressure boundary was set at the outlet of the Venturi injector and the initial pressure was set to be the same as the measured outlet pressure (p_2) in the experiment described above. Four inlet pressures (0.30, 0.35, 0.40, and 0.45 MPa) were investigated in the present study.

2.3.5 Computational Region Selection. The volume integral of the vapor phase, referred to as average V_f, was selected as the eigenvalues of cavitation in the computational domain. During simulation post-processing, two spherical volume domains were selected to compute V_f: volume–throat [with center coordinates of (0,0,0)] and volume–diffusion [with center coordinates of (28,0,0)], corresponding to the throat and diffusion portions of the Venturi injector as shown in Fig. 2. The diameters of the volume–throat and volume–diffusion domains were 30 and 60 mm, which roughly covered the experimental domains detected by the strain gauges (Fig. 3).

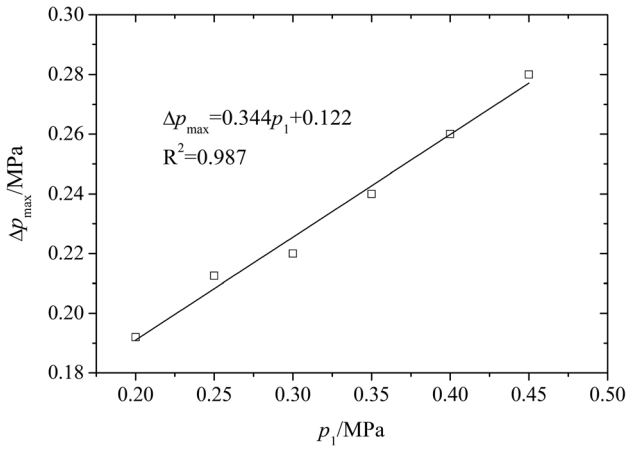

Fig. 7 Relationship between maximum pressure difference (Δp_{max}) and inlet pressure (p_1)

3 Results and Discussion

3.1 Experimental Results

3.1.1 Relationship Between SD and Δp. The SD of the measured strain values at the throat portion varied with Δp (Fig. 4). SD was relatively stable when Δp varied from 0.05 to 0.20 MPa at all inlet pressures. However, it rose sharply when Δp was greater than 0.20 MPa.

Taking the 0.45 MPa inlet pressure as an example, SD declined slightly after Δp increased to Δp_1. Afterwards, Δp continuously increased to Δp_2, and then the SD value increased rapidly. When Δp reached the value of Δp_3, the SD value began to decrease until Δp increased to its maximum measured value. In general, the SD values varied according to an M-shaped curve (Fig. 4). According to Sayyaadi's research on cavitation in Venturi reactors [30], this M-shaped effect corresponds to cavitation fluctuations in a Venturi injector, which may be caused by complex physical activity of cavitation bubbles in the injector.

Because the thickness was different between the throat and diffusion portions, and because the attachment quality and sensitivity of the strain gauges were not entirely identical, no comparison of SD values was made between the two portions. However, the change in the SD ratio SD_m/SD_1 for the two portions appeared to be very similar (Fig. 5). For an inlet pressure of 0.40 MPa, the SD_1 value was calculated at a Δp of 0.15 MPa. The values of Δp_1 and Δp_2 in the diffusion portion were in accord with those in the throat portion. When Δp varied from Δp_1 to Δp_2, the downward trend of SD in the diffusion portion was more obvious than that in the throat portion. The SD also increased when Δp became larger than Δp_2 and changed slightly at Δp_3.

3.1.2 Relationship Between SD and Q_3. The SD value in the throat portion was relatively stable, with an approximate value of 0.8 as Q_3 increased from 0 to 0.15 m^3/h (Fig. 6). It increased rapidly as Q_3 varied from 0.15 to 0.16 m^3/h. Because a smaller inlet pressure has a relatively narrower range of Δp, the measured maximum SD also became smaller. Hence, the maximum SD at an inlet pressure of 0.45 MPa was much greater than at 0.25 MPa (Fig. 6).The maximum Q_3 values for all inlet pressures were around 0.15–0.16 m^3/h (Fig. 6). This finding was similar to the results obtained by other researchers [7], which indicated that the suction flow rate did not increase, even slightly, when critical cavitation occurred in the Venturi injector. The value of SD did not rise sharply at an inlet pressure of 0.15 or 0.20 MPa (Figs. 4 and 5), which indicated that critical cavitation may not occur in the Venturi injector under these two scenarios. Therefore, an operating pressure below 0.20 MPa can be considered effective and safe for operation of the Venturi injector investigated in this study.

3.1.3 Relationship Between Δp_{max} *and* p_1. When Δp increased to a certain value, the Venturi injector began to inject fertilizer solution. The corresponding Δp and Q_1 were called the minimum pressure difference (Δp_{min}) and the minimum inlet flow rate (Q_{1min}) respectively. The suction flow rate of the Venturi injector stopped increasing and remained relatively stable at a certain value of Δp, at which the values of Δp and Q_1 were called the maximum pressure difference (Δp_{max}) and the maximum inlet flow rate (Q_{1max}), respectively, and where critical cavitation was expected to impact the flow in the Venturi injector [7]. The values of η_m [Eq. (2)] at Δp_{max} for inlet pressures of 0.30, 0.35, 0.40, and 0.45 MPa were calculated to verify the theory that Δp_{max} also corresponds to critical cavitation. In the present study, the values of η_m at Δp_{max} were approximately 20% (Fig. 5), which was greater than neighboring values and could be regarded as a criterion indicating critical cavitation.

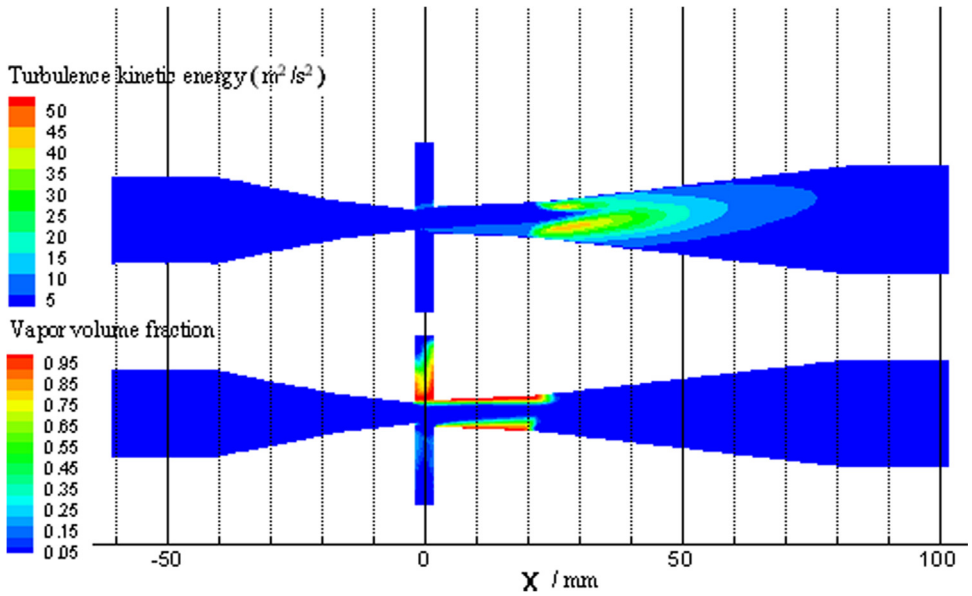

Fig. 8 Schematic diagram of internal flow in a Venturi injector for the section $Z = 0$, inlet pressure of 0.40 MPa, and outlet pressure of 0.011 MPa

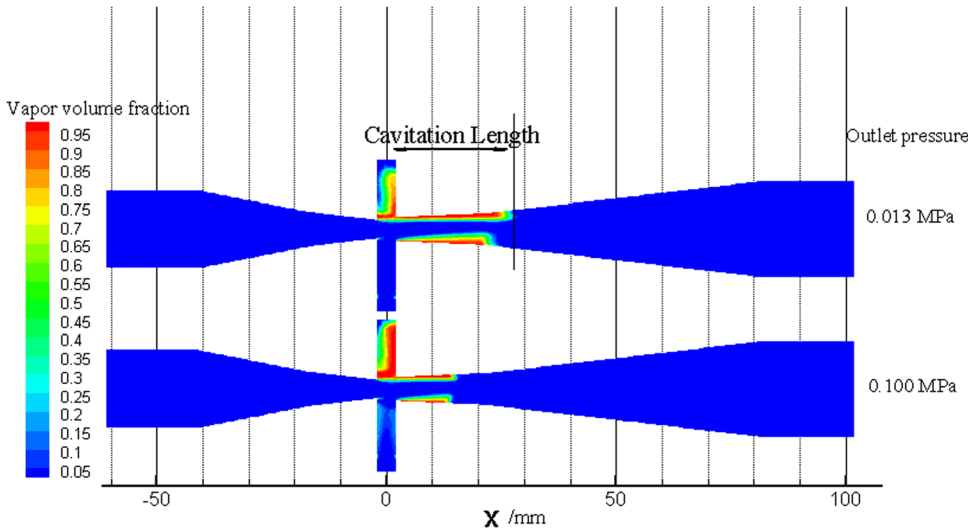

Fig. 9 Distributions of vapor-phase volume fraction (V_f) at an inlet pressure of 0.40 MPa

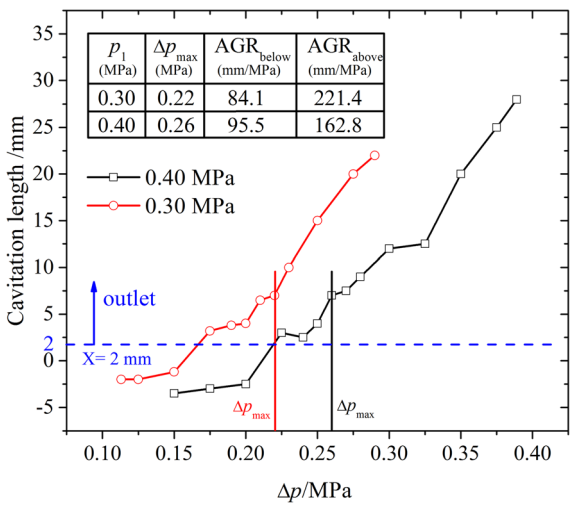

Fig. 10 Variation of cavitation length with pressure difference (Δp) at inlet pressures (p_1) of 0.40 and 0.30 MPa. The diffusion portion starts from $X = 2$ mm (dashed horizontal line).

A distinct linear relationship was found between Δp_{max} and p_1 (Fig. 7). Because no critical cavitation was observed at an inlet pressure of 0.15 MPa, the linear equation was fitted to six inlet pressures from 0.20 to 0.45 MPa. From the fitted equation, the Δp_{max} value below which the Venturi injector can operate safely without cavitation could be predicted accurately for each given inlet pressure.

3.2 Numerical Simulation

3.2.1 Internal Flow Fields. When the inlet pressure was 0.40 MPa and the outlet pressure was 0.011 MPa (Fig. 8), the turbulence kinetic energy (m^2/s^2) in the constriction portion was small, which indicated that the flow in the constriction portion was steady. The turbulence kinetic energy in the diffusion portion was relatively larger than in the throat portion because two liquid fluxes were mixing asymmetrically to form a new flux. Besides, the diameter along the diffusion portion varied, which resulted in violent turbulence in the throat and diffusion portions and larger values of turbulence kinetic energy. The flow gently slowed down near the internal tube walls of the throat and diffusion portions with relatively lower velocity and larger pressure gradient, which led to a larger vapor volume fraction (Fig. 8).

3.2.2 Cavitation Length. To explain the cavitation characteristics of the Venturi injector, the cavitation length (mm) was introduced, which was used to measure the distance between $X = 0$ and the boundary of V_f in the flow direction (Fig. 9). With an inlet pressure of 0.40 MPa, the distribution of V_f in the Venturi injector expanded from the front end of the diffusion portion to the back end as outlet pressure decreased from 0.100 to 0.013 MPa (Fig. 9).

Taking the inlet-pressure scenarios of 0.30 and 0.40 MPa as an example, the cavitation length expanded with Δp. The average growth rate of cavitation length (AGR) represents the average gradient of cavitation-length variation with Δp, AGR_{below} represents AGR between the minimum value of Δp corresponding to suction initiation (Δp_{min}) and Δp_{max}, and AGR_{above} represents AGR between Δp_{max} and the maximum measurable value of Δp (Fig. 10). AGR_{above} with an inlet pressure of 0.30 MPa was slightly larger than with 0.40 MPa, which means that inlet pressure might affect the value of AGR_{above}. However, for an inlet pressure of 0.40 MPa, when Δp varied from Δp_{min} (0.15 MPa) to Δp_{max} (0.26 MPa), AGR_{below} reached a value of 95.5 mm/MPa, or 58.6% of its AGR_{above} (162.8 mm/MPa). For an inlet pressure of 0.30 MPa, AGR_{below} between Δp_{min} (0.11 MPa) and Δp_{max} (0.22 MPa) was only 84.1 mm/MPa, or 38.0% of its AGR_{above} (221.4 mm/MPa). It can be concluded that the AGR becomes much larger at pressure differences above Δp_{max}, where critical cavitation occurs.

3.3 Comparison Between SD and V_f. Taking the inlet pressure of 0.40 MPa as an example, the simulated V_f shared a similar trend with the measured SD when Δp was greater than Δp_{max} (Fig. 11). When Δp was smaller than Δp_{max}, V_f did not immediately drop to zero until Δp decreased to 0.20 MPa. However, whether or not cavitation occurs, the internal flow will always induce a certain deformation of the throat and diffusion portions. Therefore, SD at any Δp less than Δp_{max} can also be measured. In this study, all the measured SD values at pressure differences above Δp_{max} for inlet pressures of 0.30, 0.35, 0.40, and 0.45 MPa were selected and analyzed. The correlation coefficient (R^2) between the measured SD and the corresponding simulated V_f was 0.541 (Fig. 12). The relatively small R^2 might have resulted mainly from the influence of wall thickness on measured SD. According to the variations of SD and V_f in Fig. 11, the values of both η_m and AGR showed significant increases at a pressure difference of Δp_{max}. Therefore, the relationship between SD and V_f showed that cavitation detection in a Venturi injector using strain gauges was reliable.

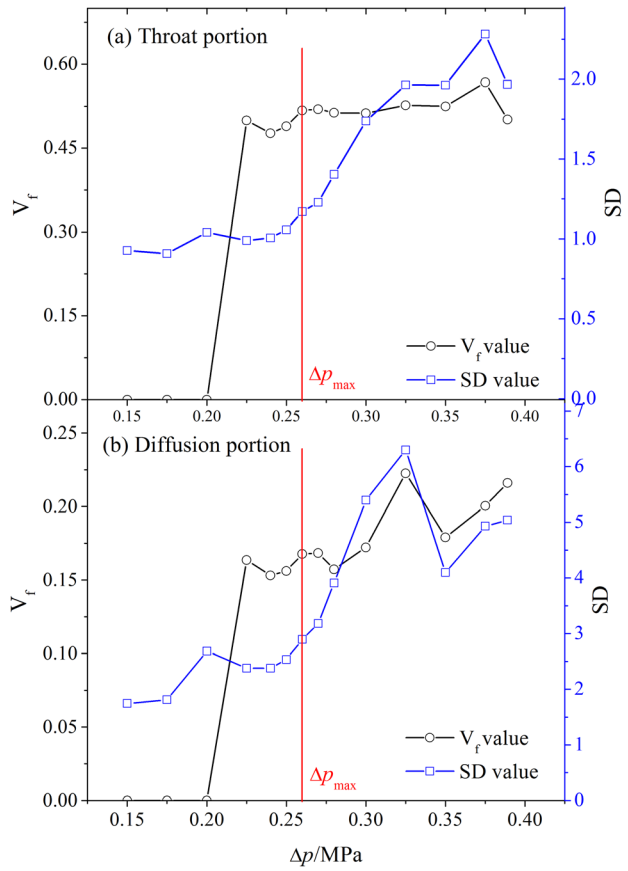

Fig. 11 Variation of simulated vapor-phase volume fraction (V_f) and SD of strain values at (*a*) the throat portion and (*b*) the diffusion portion at an inlet pressure of 0.40 MPa

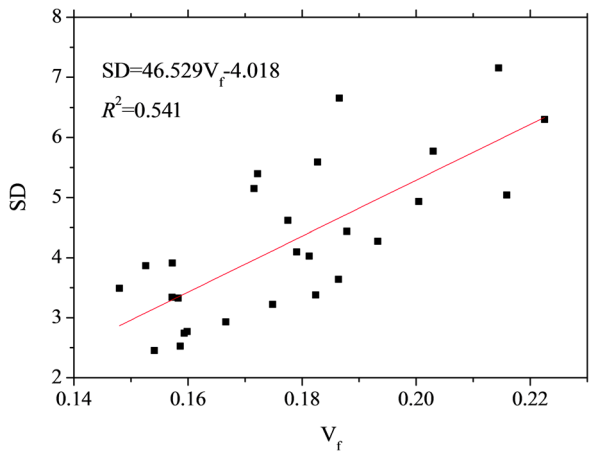

Fig. 12 Relationship between simulated vapor-phase volume fraction (V_f) and SD of strain values at inlet pressures of 0.30, 0.35, 0.40, and 0.45 MPa

4 Summary and Conclusions

In this study, both laboratory experiments and numerical simulation were conducted to test and verify a method for cavitation detection in Venturi injectors during fertilizer injection. SD was measured by strain gauges attached on the external body of the Venturi injector. Changes in SD can indicate internal flow characteristics. When critical cavitation occurred in the Venturi injector, the suction flow rate stopped increasing, and the rate of increase (η_m) of SD rose sharply, with its largest value at a pressure difference of Δp_{max} for various inlet pressures.

V_f of the internal flow in a Venturi injector was calculated to simulate cavitation using the FLUENT software. The curves of both simulated V_f and measured SD versus Δp exhibited M-shaped characteristics during the cavitation process. This M-shaped effect was presumably caused by complex physical activity of cavitation bubbles, which could indicate cavitation propagation from the throat portion into the diffusion portion. The simulated V_f for pressure differences greater than Δp_{max} agreed well with the measured SD. In addition, both the AGR of cavitation length and the value of η_m reached relatively large values at Δp_{max}. Therefore, this new method of cavitation detection in a Venturi injector using strain gauges has been verified and can be used for these fluid devices with no damage to any component or testing in complex environments.

Critical cavitation in a Venturi injector results in unstable outlet pressure and suction flow rate, which reduces fertilization uniformity in drip-irrigation systems. Therefore, determination of Δp_{max} using this method can provide a safe operating-pressure range for Venturi injectors to prevent critical cavitation.

Acknowledgment

This study has been partially supported by the Research Fund for the Doctoral Program of Higher Education of China (No. 20120008110047), the China National High Technology Research and Development Program (No. 2011AA100506), and the National Natural Science Foundation of China (No. 51321001).

Nomenclature

AGR = average growth rate of cavitation length, mm/MPa
AGR_{above} = AGR between Δp_{max} and the maximum measured value of Δp, mm/MPa
AGR_{below} = AGR between Δp_{min} and Δp_{max}, mm/MPa
d_1 = inlet diameter, m
d_3 = outlet diameter, m
p_1 = inlet pressure, MPa
p_2 = outlet pressure, MPa
Q_1 = inlet flow rate, m^3/s
Q_2 = outlet flow rate, m^3/s
Q_3 = suction flow rate, m^3/s
Q_{1max} = maximum inlet flow rate, m^3/s
Q_{1min} = minimum inlet flow rate, m^3/s
SD = standard deviation of strain values

$$SD = \sqrt{\frac{1}{n}\sum_{i=1}^{n}(\varepsilon_i - \bar{\varepsilon})^2}$$

$\bar{\varepsilon}$

ε_i

SD_1 = first SD value measured for each inlet pressure which corresponds to the start of suction
SD_j = jth SD value
V_f = simulated vapor-phase volume fraction
Δp = difference between p_1 and p_2, MPa
Δp_1 = first eigenvalue of pressure difference, MPa
Δp_2 = second eigenvalue of pressure difference, MPa
Δp_3 = third eigenvalue of pressure difference, MPa
Δp_{max} = maximum pressure difference corresponding to maximum suction flow rate, MPa
Δp_{min} = minimum pressure difference corresponding to start of suction, MPa
$\bar{\varepsilon}$ = average strain values in a period of 20 s
ε_i = ith strain value in 20 s
η_m = rate of increase of average SD

$$\eta_m = \frac{SD_m - \frac{1}{m-1}\sum_{j=1}^{m-1} SD_j}{\frac{1}{m-1}\sum_{j=1}^{m-1} SD_j} \times 100\%$$

SD_j

$v_1 =$ inlet velocity, m/s
$v_1 = 4Q_1/(\pi d_1^2)$
$Q_1, \mathrm{m}^3/\mathrm{s}$
d_1, m

$v_3 =$ suction velocity, m/s
$v_3 = 4Q_3/(\pi d_3^2)$
$Q_3, \mathrm{m}^3/\mathrm{s}$
d_3, m

References

[1] MWR, 2012, *2011 Statistic Bulletin on China Water Activities*, China Water Power Press, Beijing (in Chinese).
[2] Bar-Yosef, B., 1999, *Advances in Fertigation, Advances in Agronomy*, Elsevier Academic, San Diego, CA.
[3] Goldberg, D. G. B., and Rimon, D., 1976, *Drip Irrigation: Principles, Design and Agricultural Practice*., Drip Irrigation Scientific, New York.
[4] Schwankl, L., 2001, *Fertigation and Injection Systems, Drip Irrigation for Row Crops*, New Mexico State University, Las Cruces, NM.
[5] Kedrinskii, V. K., 1976, "Negative-Pressure Profile in Cavitation Zone at Underwater Explosion Near Free-Surface," Acta Astronaut., **3**(7–8), pp. 623–632.
[6] Jin, Y. K., Xia, C. H., and Fang, B. L., 2006, "Research and Development of Venturi Fertilizer Applicator Series," China Rural Water and Hydropower, **5**, pp. 14–16.
[7] Yan, H. J., Chu, X. Y., Wang, M., and Wang, Z. Y., 2010, "Injection Performance of Venturi Injector in Micro-Irrigation System," J. Drain. Irrig. Mach. Eng., **28**(3), pp. 251–255.
[8] Barre, S., Rolland, J., Boitel, G., Goncalves, E., and Patella, R. F., 2009, "Experiments and Modeling of Cavitating Flows in Venturi: Attached Sheet Cavitation," Eur. J. Mech. B/Fluids, **28**(3), pp. 444–464.
[9] Ardiansyah, T., Takahashi, M., Asaba, M., and Miura, K., 2011, "Cavitation Damage in Flowing Liquid Sodium Using Venturi Test Section," J. Power Energy Syst., **5**(1), pp. 77–85.
[10] Cudina, M., 2003, "Detection of Cavitation Phenomenon in a Centrifugal Pump Using Audible Sound," Mech. Syst. Signal Pr., **17**(6), pp. 1335–1347.
[11] Cudina, M., and Prezelj, J., 2009, "Detection of Cavitation in Operation of Kinetic Pumps. Use of Discrete Frequency Tone in Audible Spectra," Appl. Acoust., **70**(4), pp. 540–546.
[12] Pu, Z. Q., Zhang, W., Shi, K. R., and Wu, Y. L., 2005, "Research on Turbine Cavitation Testing Based on Wavelet Singularity Detection," Proc. CSEE, **25**(8), pp. 105–109.
[13] Liu, Y., He, Y. Y., and Chen, D. R., 2009, "Wavelet Entropy Based Condition Test and Identification of Cavitation," J. Mech. Strength, **31**(1), pp. 19–23.
[14] Al-Hashmi, S. A., 2009, "Statistical Analysis of Vibration Signals for Cavitation Detection," IEEE Symposium on Industrial Electronics and Applications, Kuala Lumpur, Malaysia.
[15] Yazici, B., Tuncer, I. H., and Ali Ak, M., 2007, "Numerical & Experimental Investigation of Flow Through a Cavitating Venturi," 3rd International Conference on Recent Advances in Space Technologies, Istanbul, Turkey.
[16] Maekawa, A., Shimizu, Y., Suzuki, M., and Fujita, K., 2005, "Experimental Study of Coupling Vibration Characteristics Between a Thin Cylindrical Water Storage Tank and Its Contained Liquid," Proceedings of the ASME Pressure Vessels and Piping Conference, Denver, CO, July 17–21, pp. 113–120.
[17] Zhang, C., Pettigrew, M. J., and Mureithi, N. W., 2006, "Correlation Between Vibration Excitation Forces and the Dynamic Characteristics of Two-Phase Flow in a Rotated Triangular Tube Bundle," Proceedings of the ASME Pressure Vessels and Piping Conference, Vancouver, Canada, July 23–27, pp. 325–334.
[18] Inaba, K., and Shepherd, J. E., 2010, "Dynamics of Cavitating Flow and Flexural Waves in Fluid-Filled Tubes Subject to Axial Impact," Proceedings of the ASME Pressure Vessels and Piping Conference, Bellevue, Washington, July 18–22, pp. 89–98.
[19] Coutier-Delgosha, O., Reboud, J. L., and Delannoy, Y., 2003, "Numerical Simulation of the Unsteady Behaviour of Cavitating Flows," Int. J. Numer. Methods Fluids, **42**, pp. 527–548.
[20] Dittakavi, N., Chunekar, A., and Frankel, S., 2010, "Large Eddy Simulation of Turbulent-Cavitation Interactions in a Venturi Nozzle," ASME J. Fluids Eng., **132**(12), p. 121301.
[21] Mejri, I., Bakir, F., Rey, R., and Belamri, T., 2006, "Comparison of Computational Results Obtained From a Homogeneous Cavitation Model With Experimental Investigations of Three Inducers," ASME J. Fluids Eng., **128**(6), pp. 1308–1323.
[22] Nouri, N. M., Moghimi, M., and Mirsaeedi, S. M. H., 2010, "Large Eddy Simulation of Natural Cavitating Flows in Venturi-Type Sections," J. Mech. Eng. Sci., **225**(2), pp. 369–381.
[23] Yan, H. J., and Chu, X. Y., 2011, "Numerical Simulation for Influence of Throat Diameter on Venturi Injector Performance," J. Drain. Irrig. Mach. Eng., **29**(4), pp. 359–363.
[24] Launder, B. E., and Spalding, D. B., 1972, *Lectures in Mathematical Models of Turbulence*, Academic Press, London.
[25] Schnerr, G. H., and Sauer, J., 2001, "Physical and Numerical Modeling of Unsteady Cavitation Dynamics," Fourth International Conference on Multiphase Flow, New Orleans, LA, May 27–June 1.
[26] Singhal, A. K., Athavale, M. M., Li, H., and Jiang, Y., 2002, "Mathematical Basis and Validation of the Full Cavitation Model," ASME J. Fluids Eng., **124**(3), pp. 617–624.
[27] Philip, J., Zwart, A. G. G., and Belamri, T., 2004, "A Two-Phase Flow Model for Predicting Cavitation Dynamics," International Conference on Multiphase Flow, Yokohama, Japan.
[28] Yuan, W., Günter, J. S., and Schnerr, H., 2001, "Modeling and Computation of Unsteady Cavitation Flows in Injection Nozzles," Méc. Ind., **2**(5), pp. 383–394.
[29] Kozubkova, M., and Rautova, J., 2009, "Cavitation Modeling of the Flow in Laval Nozzle," 3rd IAHR International Meeting of the Workgroup on Cavitation and Dynamic Problems in Hydraulic Machinery and Systems, Czech Republic.
[30] Sayyaadi, H., 2010, "Instability of the Cavitating Flow in a Venturi Reactor," Fluid Dyn. Res., **42**(5), p. 055503.